Draft version March 23, 2018
Preprint typeset using LaTeX style emulateapj v. 01/23/15

ESTIMATING THE THICKNESS OF THE H II REGIONS G031.727+0.698 AND G034.133+0.471

Nihan Pol
Department of Physics and Astronomy, West Virginia University, Morgantown, WV, USA
Draft version March 23, 2018

ABSTRACT

We present a new method to calculate the thickness of an H II region using radio recombination line observations. This method is independent of the distance to the H II region, and can be applied generally to H II regions where the distance measurement is highly uncertain. We give a demonstration of this method using the Galactic H II regions G031.727+0.698 and G034.133+0.471, and measure a thickness of 0.74×10^{-3} pc and 82.31×10^{-3} pc respectively. We discuss the implications of this thickness, and the applicability of our method.

1. INTRODUCTION

High-mass star formation occurs in dense molecular clouds in the spiral arms of the Galaxy. The bright UV emission from these high-mass stars ionizes the gas in the environment of these stars. The gas around these stars is mainly composed of hydrogen, and once this is ionized, gives rise to H II regions. Because these stars have short lifetimes ($\sim$ 10 Myr), the H II regions are used to trace the present star formation in the Galaxy.

Recently, an analysis carried out by Anderson *et al.* (2011) with the Green Bank Telescop (GBT) nearly doubled the number of known H II regions in the Galaxy. They detected 603 discrete hydrogen radio recombination line (RRL) components at 9 GHz from 448 sources. The structure of these H II regions is assumed to be a Strömgren sphere (Strömgren 1939). As such, the radius of these regions measured using their angular diameter was assumed to represent the thickness of these H II regions. In this work, we explore a method to measure the thickness of these H II regions independent of the angular diameter of these sources. We can do this by using the line brightness temperature measured for the RRLs observed from these regions along with the electron temperature in the H II regions.

To demonstrate this method, we use two H II regions from the catalog published by Anderson *et al.* (2011), G031.727+0.698 (hereafter G031) and G034.133+0.471 (hereafter G034). G031 is a faint H II region that is barely visible in the RRL data, while G034 is a relatively bright H II region, clearly visible in the RRL data. Using these two sources, we can demonstrate that our method to calculate the thickness of the H II regions can be applied generally to all H II regions, provided that they can be detected in RRL with any telescope.

In Sec. 2, we describe the data from Anderson *et al.* (2011) corresponding to G031 and G034. In Sec. 3 we describe the method to calculate the thickness of H II regions and the results from that analysis corresponding to G031 and G034. In Sec. 4 we discuss the implications of the results and the applicability of our method, and offer the conclusion in Sec. 5.

2. H II REGION DATA

For this analysis, we use data from the H II Region Discovery Survey (HRDS, Anderson *et al.* 2011). These data were collected using the 100 m Green Bank Telescope (GBT) at 9 GHz (3 cm). These data consist of continuum scan and radio recombination line (RRL) information for each H II source in the HRDS catalog. The RRL data represent the average of spectral lines from H87α to H93α, which is done to improve the signal-to-noise ration of the RRL (Balser 2006).

From this HRDS catalog, we extract the RRL data corresponding to the H II regions G031 and G034. We also extract one continuum scan in order to measure the beamwidth of the GBT at X-band frequencies (8–10 GHz), and subsequently calculate the aperture efficiency and effective area of the GBT for these observations. These data were available as ASCII text files, with the continuum scan data containing right ascension (RA) and antenna temperature (T_a) and the RRL data for each source consisting of frequency (in units of MHz) and antenna temperature. The continuum scan and RRL data for G031 are plotted in Fig. 1 and Fig. 2 respectively.

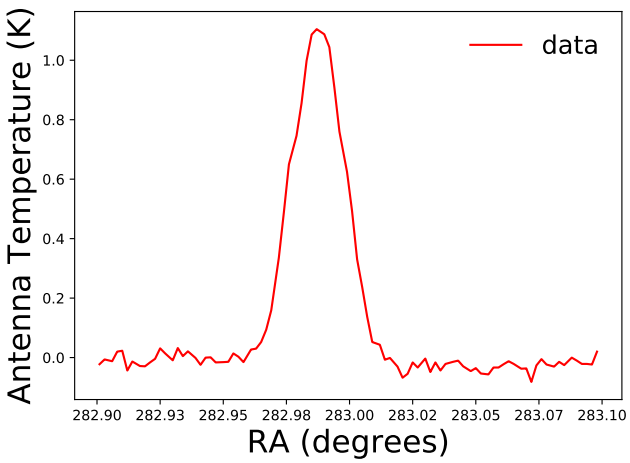

Figure 1. Data for the continuum scan of the sky. The graph plots the antenna temperature in Kelvin as the telescope slews over the target source. The Gaussian shape of the beam implies that the observed source is a point-like source.

The RRL data for G031 was severely affected by baseline irregularities. The raw data for G031 is shown in the top panel of Fig. 2. To remove the baseline irregularity, we fit a third-order polynomial to the entire data and subtracted that polynomial from the data. This re-

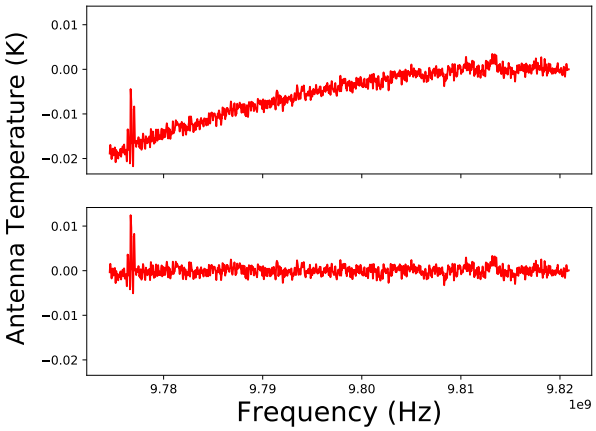

Figure 2. Radio recombination line data for G031. The top panel shows the raw data obtained from Anderson *et al.* (2011), which is severly affected by baseline irregularity. We fit a third-order polynomial to the baseline to remove the irregularity. The corrected data is shown in the bottom panel. This corrected data is used in further analyses. The feature around 9.78 GHz is radio frequency interference (RFI).

moved the baseline irregularities, which can be seen in the bottom panel of Fig. 2. The RRL for G031 is also very weak, and had to be located by eye. The RRL for G034 was sufficiently bright to be clearly visible in the data (see Fig. 4).

3. DATA ANALYSIS AND RESULTS

To calculate the source thickness, we need to calculate the electron temperature in the H II region and the RRL brightness temperature using the data obtained in Sec. 2. All of the analysis was done in Python.

3.1. *Effective area and aperture efficiency*

Before we can do that, we need to estimate the aperture efficiency for the GBT for these observations. To calculate this value, we fit a Gaussian curve to the continuum scan shown in Fig. 3. The standard deviation, σ, of the best-fit Gaussian can be converted to the full-width at half of maximum (FWHM), $\theta_{\rm FWHM}$,

$$\theta_{\rm FWMH} = 2.355 \times \sigma \tag{1}$$

The FWHM in this case corresponds to the size of the beam of the GBT in degrees. Using the FWHM, we can calculate the effective diameter of the dish, $D_{\rm eff}$,

$$\theta_{\rm FWHM} = \frac{c}{\nu\, D_{\rm eff}} \tag{2}$$

where ν is the central observation frequency, which in this case is 9 GHz. With the effective diameter, we can calculate the effective area, $A_{\rm eff}$, and consequently, the aperture efficiency, $\eta_{\rm A}$,

$$\eta_{\rm A} = \frac{A_{\rm eff}}{A_{\rm geom}} = \frac{\pi\, D_{\rm eff}^2/4}{\pi\, D_{\rm geom}^2/4} \tag{3}$$

where $A_{\rm geom}$ and $D_{\rm geom}$ are the geometric area and diamter (100 m) of the GBT dish respectively. Using the FWHM obtained from the continuum scan, we calculate an effective area $A_{\rm eff} = 5262.97$ m^2 and an aperture efficiency $\eta_{\rm A} = 0.67$.

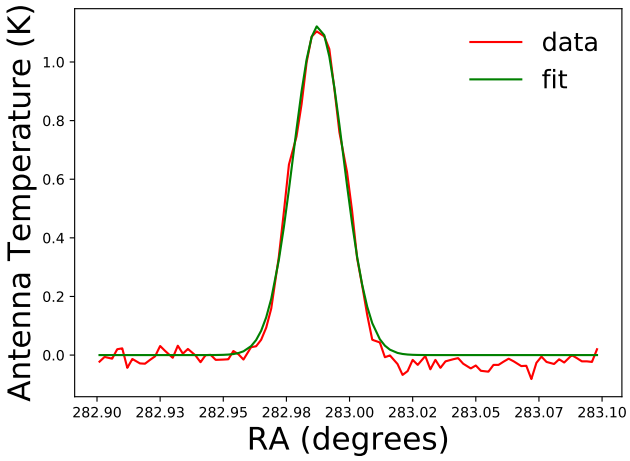

Figure 3. Best-fit Gaussian curve to the beam from the continuum scan. The errors on the Gaussian fit are negligible compared to the best-fit value.

3.2. *Electron temperature*

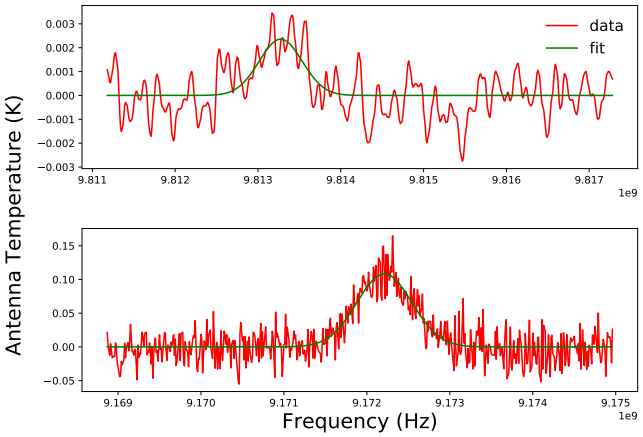

Figure 4. Best-fit Gaussian curves for the radio recombination line data. The top panel shows the best-fit Gaussian for G031, while the bottom panel shows the best-fit Gaussian for G034. The errors on the Gaussian fits are negligible compared to the best-fit parameters. We can also see the difference in the signal-to-noise ratio of the lines from G031 and G034.

We can calculate the electron temperature in the H II regions using the RRL data. We fit a Gaussian curve to the RRL observed in the data for both H II regions G031 and G034, shown in Fig. 4. Using Eq. 1, we calculate the corresponding FWHM for the best-fit Gaussian curves. In this case, the FWHM corresponds to the line width, $\Delta\nu$, while the mean of the Gaussian corresponds to the peak frequency of the RRL, ν_0.

The electron temperature, T_e in the H II regions can be calculated using Eq. 7.35 in Essential Radio Astronomy (ERA, Condon and Ransom 2016),

$$\Delta\nu = \left[\frac{8\ln(2)\,k}{c^2}\right]^{1/2} \left(\frac{T_e}{M_H}\right)^{1/2} \nu_0 \tag{4}$$

where k is the Stefan-Boltzmann constant and M_H is the mass of hydrogen atom.

3.3. *Line brightness temperature*

To calculate the line brightness temperature, T_b, we need to obtain a relation between the antenna temperature, which is obtained from the GBT data, with the brightness temperature. To do this, we first define the flux from a source, S_ν as,

$$I_\nu = \frac{S_\nu}{\Omega} = \frac{2\,k\,T_b\,\nu^2}{c^2} \tag{5}$$

where I_ν is the intensity of the source at a frequency ν, and Ω is solid angle subtended by the beam on the sky. The beam solid angle, Ω, can be calculated using the FWHM of the beam size obtained in the continuum scan and Eq. 3.118 from ERA (Condon and Ransom 2016),

$$\Omega = 1.113 \times \theta^2_{\rm FWHM} \tag{6}$$

However, the flux, S_ν can be related to the antenna temperature T_a of the telescope by Eq. 3.48 from ERA,

$$T_a = \frac{A_e\,S_\nu}{2\,k} \tag{7}$$

where A_e is the effective area of the telescope, calculated in Sec. 3.1.

Combining Eq. 5, Eq. 6, and Eq. 7 to solve for the brightness temperature in terms of the antenna temperature, we get,

$$T_b = \frac{T_a\,c^2}{A_e\,\Omega\,\nu^2} \tag{8}$$

where ν is the center frequency of the observed RRL.

The calculated electron temperatures and line brightness temperature for G031 and G034 are listed in Table 1.

	G031	G034
Electron temperature (K)	9362	14 367
Line brightness temperature (K)	2.3×10^{-3}	0.12
Emission measure (pc cm^{-6})	738	82 313
Thickness (pc)	0.74×10^{-3}	82.31×10^{-3}
Radius (pc)	4.0	2.4

Table 1
The results from the calculations carried out in our analysis.

3.4. *Thickness of* H II *regions*

Using the line brightness temperature, T_b, and the electron temperature, T_e, we can calculate the emission measure (EM) of the H II regions, assuming that they are optically thin, i.e. the optical depth $\tau \ll 1$, using Eq. 7.97 from ERA,

$$T_b = 1.92 \times 10^3 \left(\frac{T_e}{\rm K}^{-3/2}\right) \left(\frac{\rm EM}{\rm pc\,cm^{-6}}\right) \left(\frac{\Delta\nu}{\rm kHz}^{-1}\right) \tag{9}$$

The emission measures for G031 and G034 are listed in Table 1.

Using the definition of the emission measure, we can try to estimate the thickness of the source of emission measure,

$$\rm EM = \int_{los} \left(\frac{n_e}{cm^{-3}}^2\right) d\left(\frac{s}{pc}\right) \tag{10}$$

where n_e is the electron density along the line of sight (los) and ds is the infinitesimal path length along the line of sight. If we assume that the emission measure contribution along the line of sight is negligible compared to that of the H II region, and assume that the emission measure of the source is constant, then the integral in the above equation equation can be removed, and the equation modified to obtain a source thickness,

$$\frac{S}{\rm pc} = \frac{\rm EM}{n_e^2} \tag{11}$$

Assuming a free electron density, $n_e = 10^3$ cm^{-3}, the measured thickness of G031 and G034 is listed in Table 1.

The Python code for all of the above analysis is available on the GitHub page for this project[1].

4. DISCUSSION

We list the thickness of the H II regions as calculated from the emission measure in Table 1. We can also calculate the radius, r, of these H II regions by using the measured distance to the source, D, and the angular radius, θ, of the source subtended on the sky,

$$r = D \times \theta \tag{12}$$

The radii of G031 and G034 are listed in Table 1.

Comparing the apparent radius of the H II regions with their thickness, we can see that they are quite different from each other. In fact, the thickness of G031 is only ∼0.02% of the radius, while the thickness of G034 is ∼3.4% of the radius. This demonstrates significant deviation from the assumption of H II regions being Strömgren spheres (Strömgren 1939) where the diamter of the H II regions is equal to the thickness of the region. This hints towards the existence of other physical processes that might introduce asymmetries in the observed H II region.

One possible reason for this asymmetry might be due to the motion of the stars responsible for the creation of these H II regions. Both the H II regions analyzed here have similar velocities $V_{\rm LSR} \sim 35$ km/s. While these velocities are modest, they are not the largest measured velocities for H II regions, which might make this line of reasoning not applicable for this case.

Another reason for the asymmetry could be radiation pressure from surrounding stars in the cluster. The location of the G031 region is consistent with a star forming cluster, as can be seen from the WISE Catalog of Galactic H II regions[2]. Usually, the radiation pressure is negligible compared to the gas pressure for isolated H II regions. However, the presence of other young stars around the H II region G031 could be suppressing the expansion of the H II regions in some directions and thus introducing an asymmetry in the observed H II region.

Finally, this type of measurement of an H II region thickness might not be an accurate representation of the true thickness of the entire H II region. Our assumption

[1] https://github.com/NihanPol/radio_astronomy_project1
[2] http://astro.phys.wvu.edu/wise/

of the free electron density, $n_e = 10^3$ cm^{-3}, might be inaccurate for these H II regions. A more detailed analysis of multiple emission lines, especially molecular emission lines might return an accurate value for the free electron density. This analysis was also based on the assumption that the entire H II region is transparent ($\tau \ll 1$). However, this might not be accurate, and it is possible that we are only observing emission from the side of the H II region facing us, while we are insensitive to the emission from the opposite face of the H II region. This implies the measured antenna temperature T_a is lower than it would be if we were observing both faces of the H II region. This in turn implies that we are calculating a lower line brightness temperature T_b, which would result in a lower measured source thickness. A similar analysis with other H II regions is necessary to determine the applicability of this type of analysis to measure the thickness of H II regions.

5. CONCLUSION

We demonstrate a method to calculate the thickness of H II regions using radio recombination lines. We measured a thickness of 0.74×10^{-3} pc and 82.31×10^{-3} pc for the H II regions G031 and G034 respectively. We show that these thickness measurements are much smaller than the radius of the H II regions, which is contrary to the standard assumption of Strömgren sphere where the thickness is equal to the radius of the H II region.

We explore some physical processes that might give rise to this deviation from a Strömgren sphere, and show that they do not completely explain the dramatic differences in radius and thickness of the regions. We finally discuss the possibility that this method of measuring H II region thickness might not be an accurate representation of the true thickness of the region. Analysis of other H II regions with this method will help determine if this method is an accurate representation of H II region thickness or not.

REFERENCES

L. D. Anderson, T. M. Bania, D. S. Balser, and R. T. Rood, The Astrophysical Journal Supplement Series **194**, 32 (2011).
B. Strömgren, ApJ **89**, 526 (1939).
D. S. Balser, AJ **132**, 2326 (2006), astro-ph/0608436.
J. J. Condon and S. M. Ransom, *Essential Radio Astronomy, by James J. Condon and Scott M. Ransom. ISBN: 978-0-691-13779-7. Princeton, NJ: Princeton University Press, 2016.* (2016)